Electronic Supplementary Material (ESI) for Chemical Communications.

Supporting Information

Photo-triggered conversion of hydrophilic fluorescent-biomimetic nanostructure for cell imaging

Q. Dai[a, b], H. Zhao[a,*], H. Cao [a], J. Yang[d], W. Zhao[e], T. Wang [c,*], L. Liu [b ,d], Z. Fan[f], G. Wang[e]

Table of Contents

1. Experimental Section

1.1 Chemicals

Nonanoic acid (NA, ⩾97.5%) was provided by Sinopharm Chemical Reagent Co., Ltd. Acetonitrile and ethanol used in this study are of Optima LC/MS grade and were purchased from Fisher Scientific (Fair Lawn, NJ). Quinine sulfate was provided by Shanghai Macklin Biochemical Co., Ltd. Dimethyl sulfoxide (DMSO) was purchased from Xilong Scientific Co., Ltd. 3-(4,5-dimethyl-2-thiazolyl)-2,5-diphenyl-2H-tetrazolium bromide (MTT) was purchased from Sigma-Aldrich. Dulbecco's Modified Eagle Medium (DMEM), penicillin (10,000 U/mL), streptomycin (10 mg/mL), and fetal bovine serum (FBS) were obtained from Thermo. Paraformaldehyde (1% PFA) and phosphate buffered saline (PBS, pH = 7.4) were provided by Shanghai Yu Bo Biotechnology Co., Ltd. All other reagents were obtained commercially at analytical grade without further purification. Lung cancer A549 cells were purchased from Tumor Cell Bank of Chinese Academy of Medical Sciences.

1.2 Synthesis

For the preparation of fluorescent micelles, 300 ml NA/water mixture (1%, v/v) was directly poured into 500 mL round-bottom flask. Then the sample was placed in a vacuum steaming apparatus and heated under vacuum for 2 h (80 °C, ca. −0.1 MPa). Ultimately, oil-soluble fluorescent micelles were obtained. For the synthesis of fluorescent vesicles, 1% NA (v/v) was first exposed to photoirradiation ($\lambda > 254$ nm, light intensity = 12 mW/cm^2). After photoreaction for 5 h, samples were pumped into 500 mL round-bottom flask followed by being placed in a vacuum steaming device. Subsequently, these samples were steamed for 2 h under the previously same conditions. Finally, water was added to the collected sample and shaken, thus water-soluble fluorescent vesicles can be obtained and a very small number of oil-soluble fluorescent micelles were collected as the by-product. Pure FCNs from fluorescent micelles and vesicles were further separated and collected by using thin layer

chromatography silica gel plate as well as 0.22 μm microporous membrane. Petroleum ether, ethyl acetate, and acetic acid were applied as eluents (v/v/v = 18:3:3). Finally, the purified two kinds of FCNs with/without photoirradiation were dried by vacuum for structural characterization and property measurement.

1.3 Characterizations

The morphology and structure of samples were investigated through high solution field-emission transmission electron microscopy HRTEM (JEM-2100F, Japan Electronics Corp., Japan)) at an accelerating voltage of 200 kV. The samples for HRTEM characterization were prepared by placing 4~6 drops of colloidal solution on a carbon-coated copper grid and dried at ambient temperature. The size of the samples was estimated using Nanomeasurer 1.2 software. The element composition of three samples was analyzed by corresponding energy dispersive X-ray spectroscopy (EDS) with an EDS detector equipped with previously referred HRTEM. The chemical structure of FCNs was characterized using an NMR instrument (600M, AVANCE III, Bruker, Switzerland) and FT-IR (T27-Hyperion-Vector 22, Germany). The surface states and composition of the samples were measured through the X-ray photoelectron spectroscopy (XPS, ESCALAB 250Xi, Thermo Fisher Scientific, America) using Al Kα radiation at the power of 300 W. Survey and multi-region spectra were recorded at C1s and O1s photoelectron peaks. To detect the zeta potential, the products at different reaction time were diluted with water (viscosity 0.88 cP, reflection index 1.330) and determined by dynamic light scattering instrument (DLS, Zetasizer Nano ZS, UK) with 173 backscatters using water as the dispersed phase under room temperature. The samples were equilibrated for 120 seconds and tested thrice to obtain the average data. Three selected samples were detected by electron spray ionization time-of-flight mass spectrometry (ESI-TOF-MS) (Bruker, Germany) under negative mode. The mass analyzer was run at a scanning mode from m/z 100 to 1000. Nitrogen was used as desolvation gas and maintained at a flow rate of 10 L min^{-1}. The desolvation temperature was set at

350 °C. In addition, to identify vesicles composition, 1% NA was dispersed in water. After a predefined photoreaction time, samples were centrifuged at 10000 r/min for 30 min to collect the vesicles, which were subsequently diluted in acetonitrile. Then the vesicle composition was also analyzed by ESI-TOF-MS. The reaction products were verified through the following strategy in accordance with MS analysis: The molecular formulas of each species present in the reaction mixtures but not in control samples were derived from the accurately measured mass and isotope patterns. The injection volume of the sample was 5 μL.

1.4 Optical properties

The fluorescent vesicles and (b-)fluorescent micelles were dispersed in water and ethanol, respectively for the following the characterization. UV-vis absorption was measured on a UV-vis spectrophotometer (UV 9100 D, Agilent Technologies, America) using 1 cm quartz cuvettes. FL images of three samples were obtained with an UV-lamp (10 W, mercury lamp, UV-Ⅲ, Beijing BEONY Technology Co.,Ltd., China) under excitation at 365 nm. FL spectra were collected with a FL spectrometer (F-7000, Hitachi Ltd., Japan) in a 1 cm quartz cell under 3D scan and wavelength scan mode with the scan speed at 2400 nm/min. The FL lifetime of three samples was recorded on a time-resolved FL spectrometer (F-900, Edinburgh instruments, UK) under 375 nm excitation with a time correlated single photon containing (TCSPC) method. The data were deconvoluted with the instrument response function, recorded using dispersed light and fitted to a multi-exponential function. The FLQYs were determined using quinine sulfate as reference standard analyzed by UV-vis and FL spectrometer.

1.5 Cell toxicity

The cytotoxicity of fluorescent vesicles was evaluated through MTT (3-(4,5-dimethyl-2-thiazolyl)-2,5-diphenyl-2-H-tetrazolium bromide) assay. Human lung cancer cell line A549 cells were cultured

in DMEM media supplemented with 10% (v/v) fetal bovine serum (FBS) and 1% penicillin streptomycin. A549 were firstly incubated at 37 °C for 24 h in 96-well plates at a density of 5000 cells per well. After rinsing with phosphate buffered saline (PBS, pH = 7.4), A549 cells were incubated for 24 h with 200 μL of culture medium containing different concentrations (500, 250, 125, 60, 30, 15, 6.75 μg/mL) of fluorescent vesicles. Three sets of parallel replicates were prepared per concentration. Then, the medium was removed and replaced with 20 μL of MTT solution (5 mg/mL). A549 cells were further incubated for additional 3 h. Subsequently, the culture medium with MTT was discarded and replaced with 100 μL of DMSO. The plates were then shaken for 10 min. To assess the cell viability, the optical density of the mixture at 492 nm was detected by enzyme-linked immunosorbent assay using a spectrophotometer (Infinite F90, Tecan, Austria).

1.6 Cell labeling

For bioimaging, A549 cells were incubated for 24 h at 37 °C in a glass bottomed cell culture dish at a density of 5000 cells per well and then mixed with the the prepared FHVs samples. After incubation at a concentration of 250 μg/mL for 3 h, A549 cells were washed thoroughly three times with PBS (pH = 7.4) and then fixed with 1 mL of paraformaldehyde (1%, v/v). A control group was also cultured in medium without fluorescent vesicles. Glass bottom cell culture dishes were covered with tin foil until cellular images were obtained through a laser scanning confocal microscope (N-C2-SIM, Nikon instruments (Shanghai) Co., Ltd., Japan) under bright filed and three fluorescent channels (408, 488 and 561 nm, respectively)

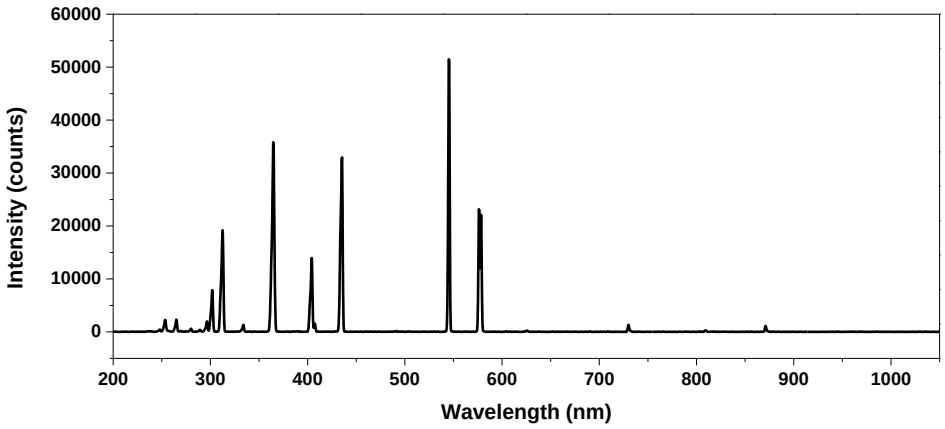

Fig. S1. Light spectrum of the lamp used in the experiment.

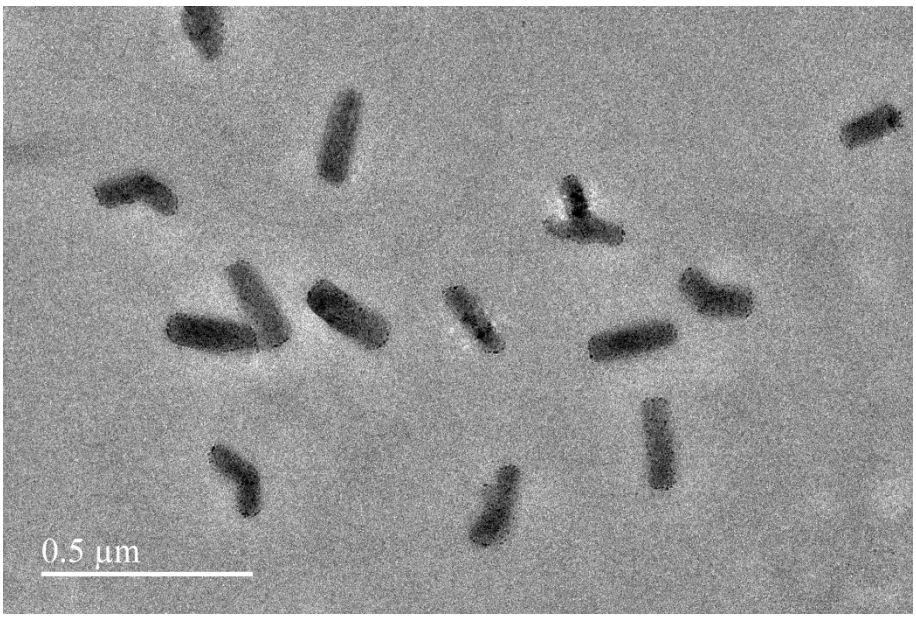

Fig. S2. TEM image of fluorescent micelles.

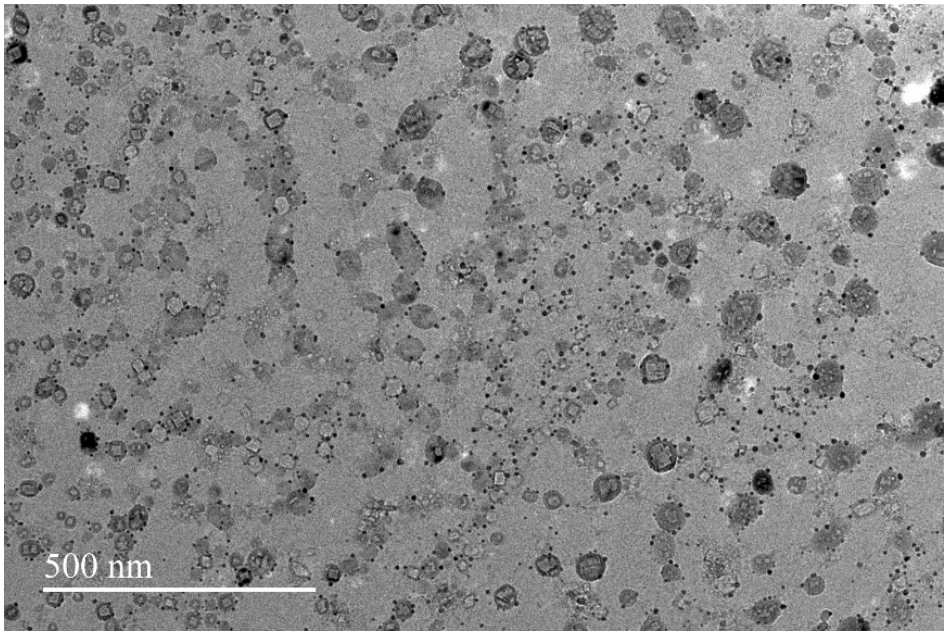

Fig. S3. TEM image of fluorescent vesicles.

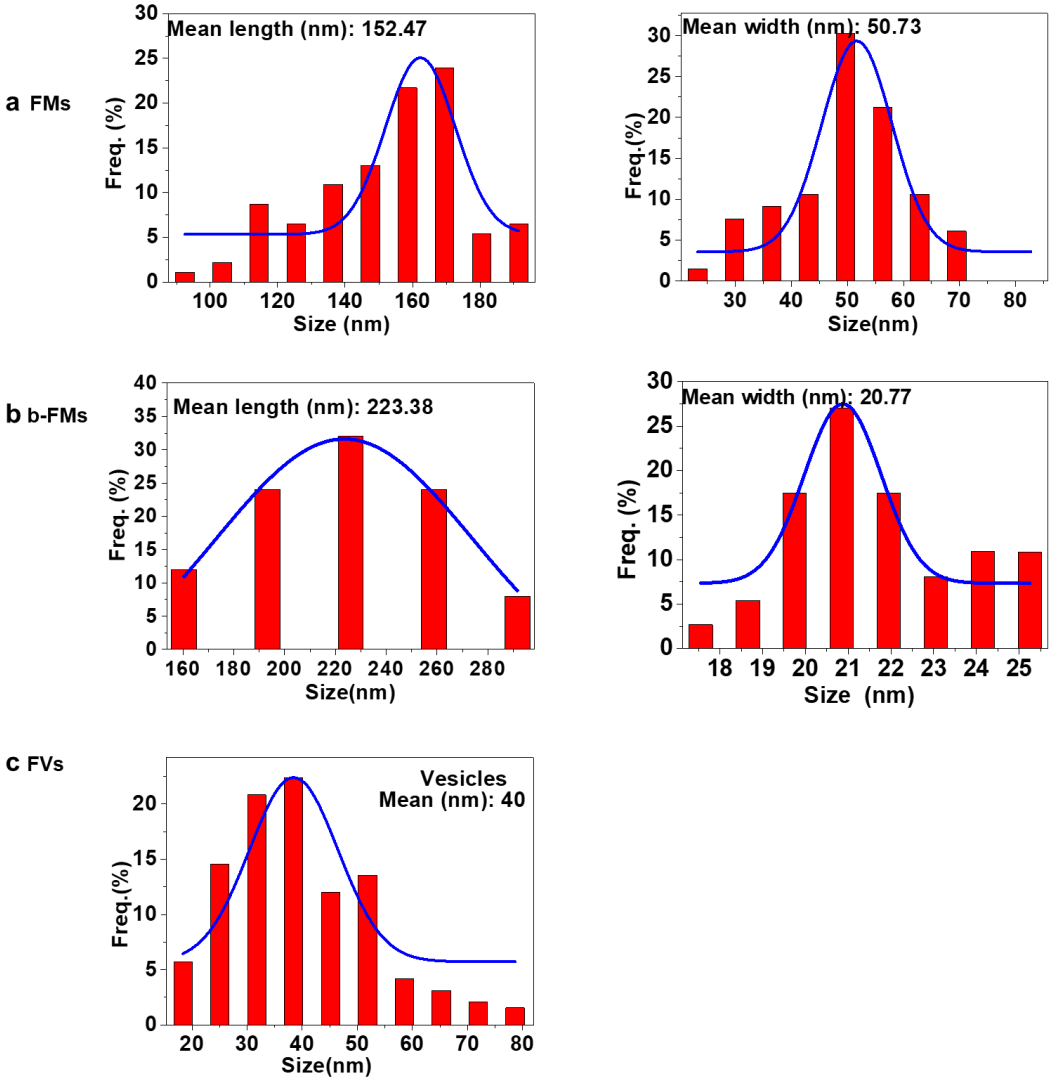

Fig. S4. The size distribution of **(a)** fluorescent micelles, **(b)** b-fluorescent micelles, and **(c)** fluorescent vesicles.

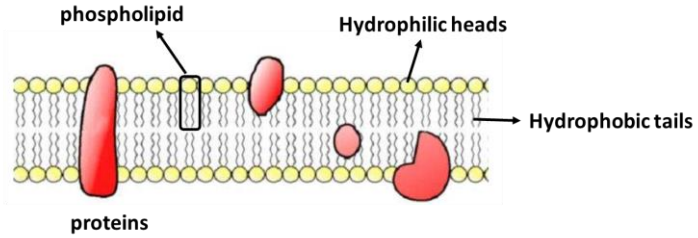

A. Schematic of cell membrane embedded with proteins

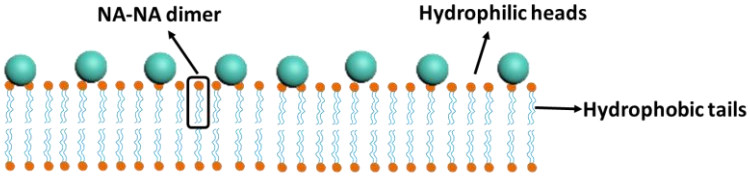

B. Schematic of fluorescent vesicles attached with FCNs

Fig. S5. Contrast diagram of cell membrane embedded with proteins (A) and vesicles attached with FCNs (B).

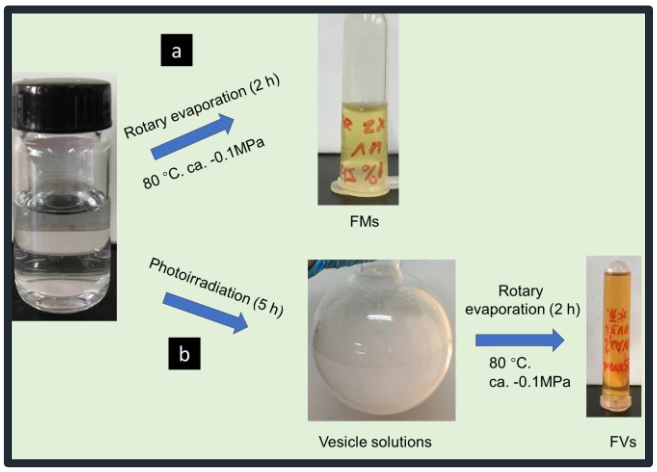

Fig. S6. Preparation process of **(a)** fluorescent micelles, **(b)** fluorescent vesicles.

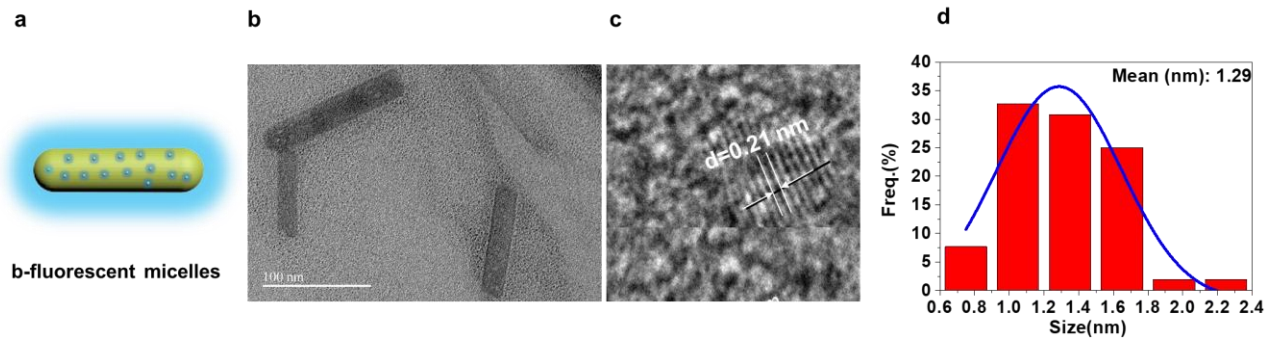

Fig. S7. Morphology characterization of b-fluorescent micelles. **(a)** the nanocomposite mode, **(b)** TEM images, **(c)** the lattice spacing, **(d)** size distribution of FCNs inserted into micelles.

As light trigger is on, a small number of fluorescent micelles were generated as by-products and were defined as b-fluorescent micelles. Oil-soluble b-fluorescent micelles were formed by the unreacted NA during rotary evaporation. Slightly different from fluorescent micelles, the b-fluorescent micelles seemed like sesame stick rather than worms. They had a length of ca. 223 nm and width of ca. 21 nm, and the ratio of length and width was ca. 11, much larger than that of fluorescent micelles. The b-fluorescent micelles were embedded with FCNs with ca. 1.3 nm and 0.21 nm lattice spacing, corresponding to the (100) facet of graphite. Compared to fluorescent micelles, the reduced diameter and changed morphology of b-fluorescent micelles were attributed to the effect of light. Both the diameters of FCNs inserted into both kinds of micelles were consistent with the previous study, where nanoparticles of sub-3nm can insert into micelles. [1]

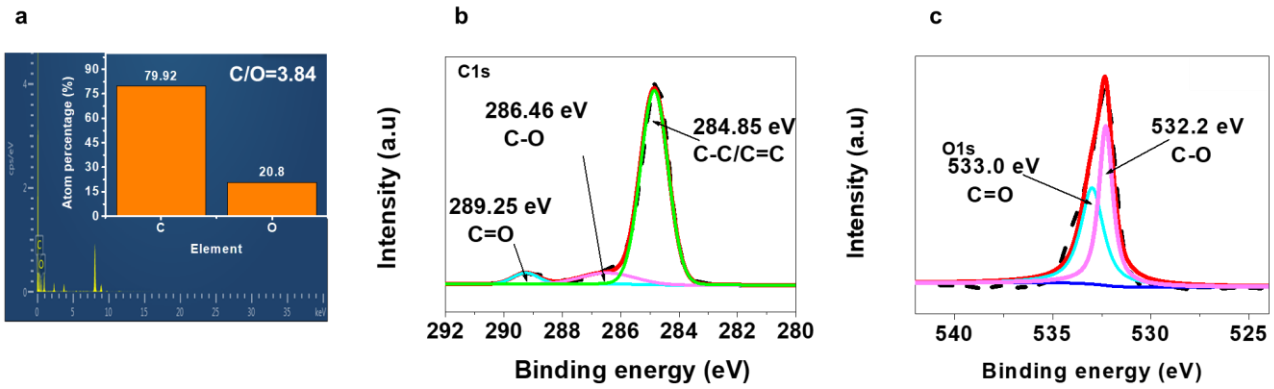

Fig. S8. Chemical structure characterization of b-fluorescent micelles. **(a)** EDS, (**b)** high-resolution XPS C1s spectra, (**c)** high-resolution XPS O1s spectra. Each band was deconvoluted following the literature.

EDS showed that the C/O ratio of the surface of b-fluorescent micelles were 3.84, smaller than that of fluorescent micelles. The reason may be attributed to the introduced additional oxygen content during photoirradiation in the atmosphere. XPS further confirmed the result. The spectra of C1s of the sample, whose four peaks at ca. 289, 286, 284.8 eV were attributed to C=O, C-O, C-C/C=C groups, [2] respectively, which mainly originated from FCNs. The C=C groups came from the core of FCNs. Different form the control group, the results demonstrated the b-fluorescent micelles were equipped with functional groups, including -COOH, -OH. The O1s spectra also verified the existence of oxygen groups, consistent with the EDS result. The oxygen content (including C=O and C-O groups) of b-fluorescent micelles was found to 14.18%, lower than that of fluorescent vesicles and higher than that of fluorescent micelles.

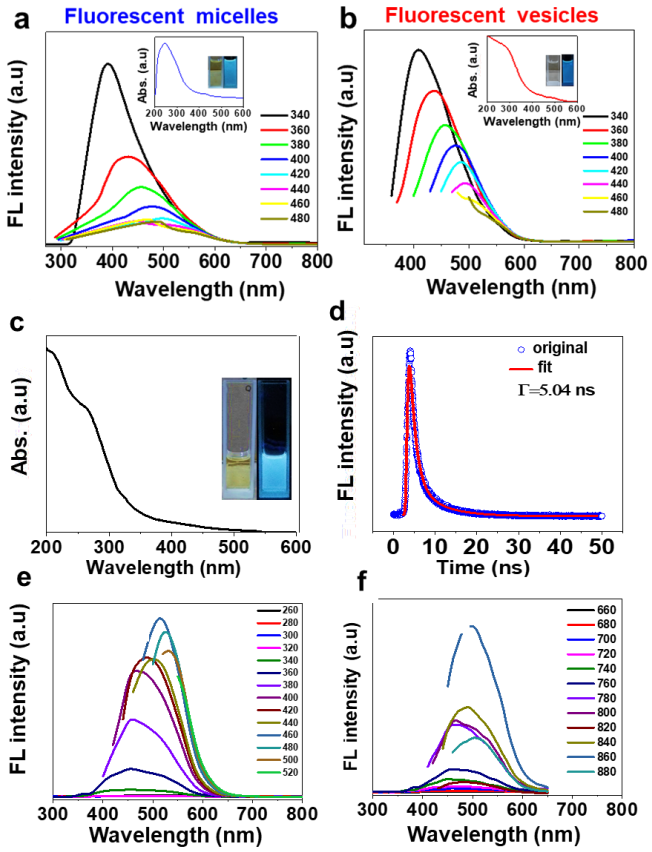

Fig. S9. Fluorescent spectra of **(a)** fluorescent micelles and **(b)** fluorescent vesicles obtained under the different excitation wavelengths showing down-conversion. Insets: UV-vis absorption spectra of fluorescent micelles and fluorescent vesicles, as well as the photographs of the sample solutions under natural daylight (left) and 365 nm UV lamp (right) irradiation. b-fluorescent micelles: **(c)** UV-vis absorption spectrum, insets are photographs of the sample solutions under room light (left) and 365-nm UV lamp (right), **(d)** FL decay spectrum under the excitation at 375 nm and emission at 450 nm, blue line represents experimental data and red line represents fitted data and corresponding lifetime value is displayed inside each graph. **(e)** down-conversion spectrum, **(f)** up-conversion spectrum.

The weak PL signal at 230 nm in the UV-vis absorption spectrum was assigned to the π-π^* transition of the aromatic sp^2 domains.[3] A shoulder at ca. 300 nm was related to the n-π^* transition of the carbonyl group (Fig. S9c-f). The prominent peaks in the visible region were ascribed to the conjugated structures that provided strong emission.[4] Previously reported FCNs exhibit absorption almost within the UV region Thus, the potential applications of the FCNs obtained in this study can be extended to photocatalysis, optoelectronic devices, and cell imaging given their strong visible absorption.[5] Under excitation at 365 nm, the emission colors of FCNs emitted blue FL. In addition to conventional down-converted photoluminescence emission, FCNs possessed up-converted FL emission properties.[6] Up-converted PL is particularly attractive for *in vivo* bioimaging because long wavelengths, especially in the NIR region are usually preferred for bioimaging given that they improve photon tissue penetration and reduce background auto-FL.[5] b-fluorescent micelles can be excited over a wide wavelength range and provided well-defined maximum emission peaks. Besides, compared to fluorescent micelles and vesicles, b-fluorescent micelles have shortest fluorescent life time with 5.04 ns, which may be due to the smallest diameter of FCNs inserted its interior.

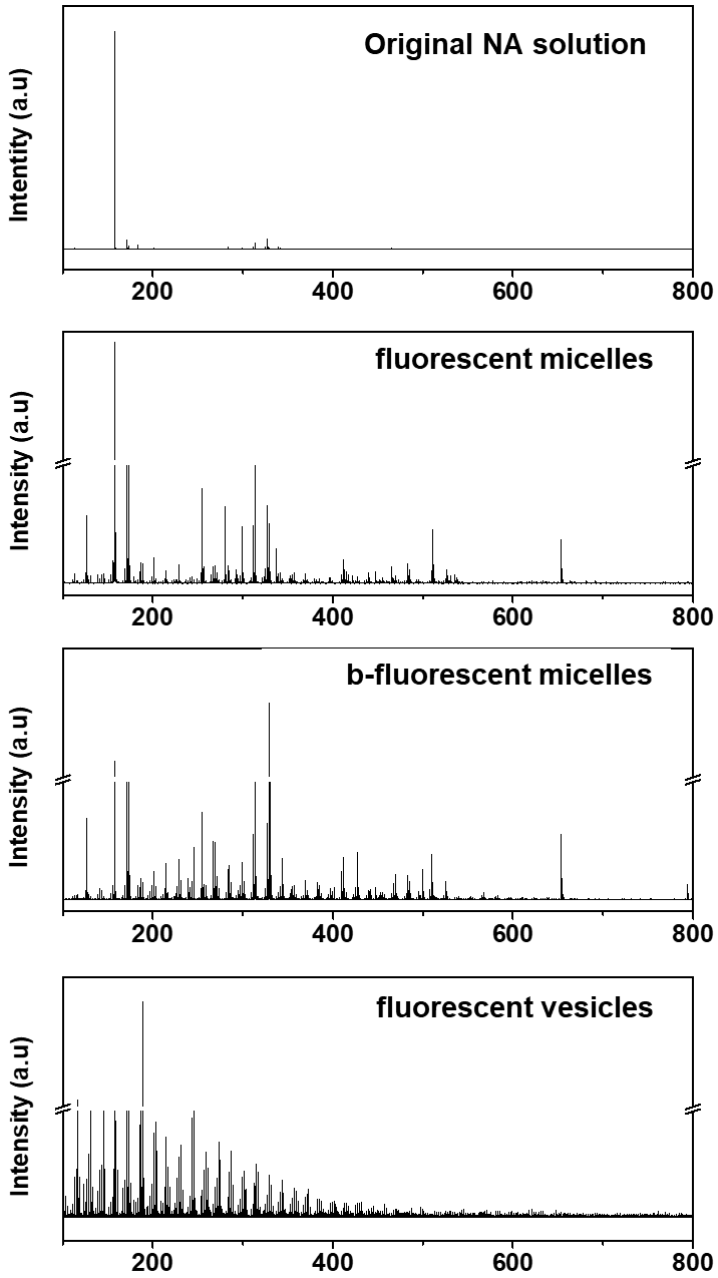

Fig. S10. Mass spectra of NA, fluorescent micelles, b-fluorescent micelles and vesicles detected under negative mode.

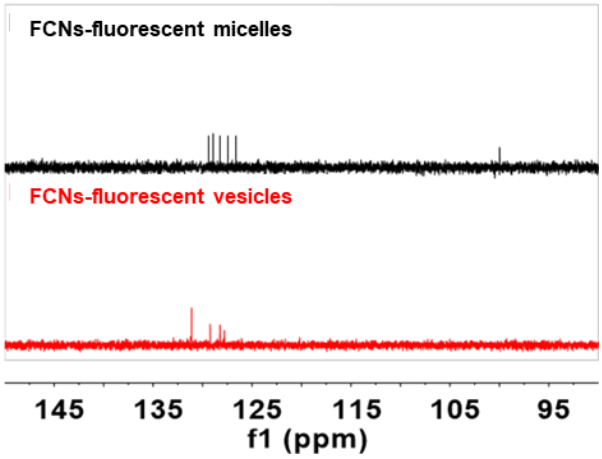

Fig. S11. ^{13}C NMR spectra of FCNs from fluorescent micelles (black line) and fluorescent vesicles (red line).

a

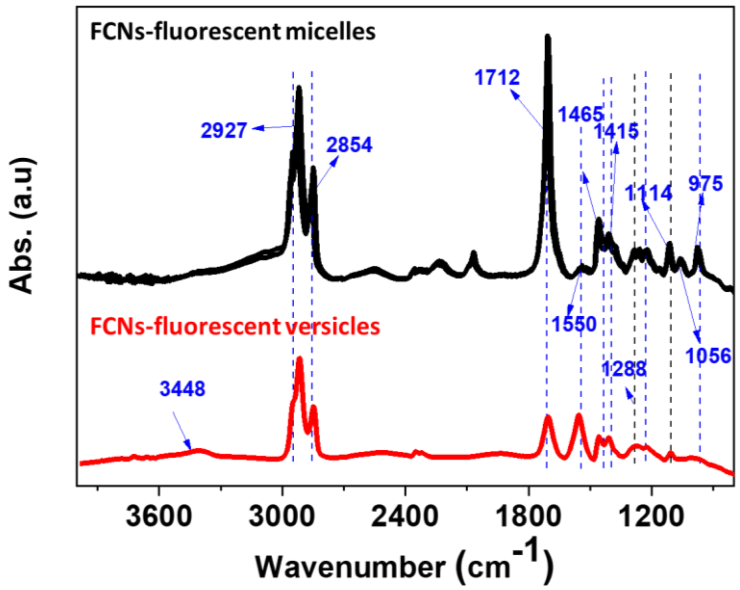

b

Wavenumber （cm^{-1}）	Probable assignment
3421	O-H (stretch)
2927	C-H (stretch)
2854	C-H (stretch)
1712	C=O
1550	C=C
1462	C=C
1415	C=C
1288	C-O
1114	C-O-C
975	Ar-H

Fig. S12. **(a)** FT-IR spectra of FCNs from fluorescent micelles (black line) and fluorescent vesicles (red line) and **(b)** Labeling of peaks in FTIR spectra.

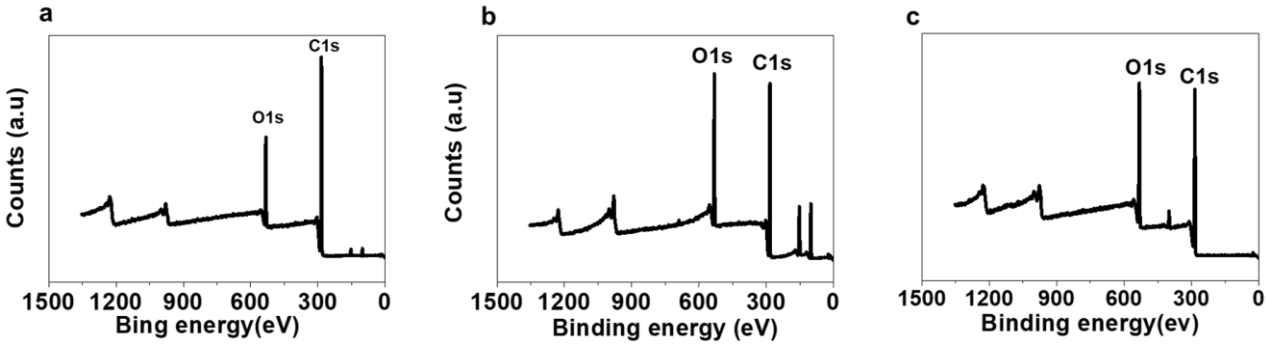

d

sample	C-O (%)	C=O (%)	C-C/C=C (%)
fluorescent micelles	0	0	100
b-Fluorescent micelles	9.56	4.62	85.82
fluorescent vesicles	29.60	10.42	59.98

Fig. S13. XPS spectra of **(a)** fluorescent micelles, **(b)** b-fluorescent micelles, and **(c)** fluorescent vesicles. **(d)** XPS data analyses of the C1s spectra of three fluorescent nanocomposites.

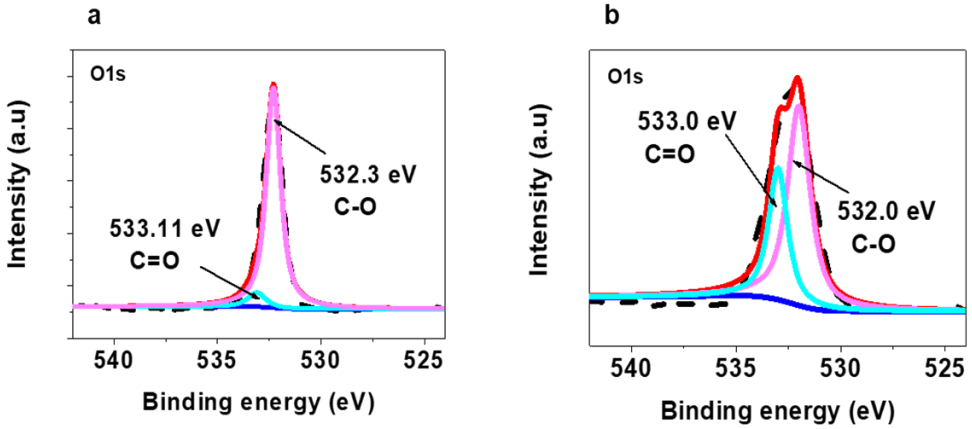

Fig. S14. High-resolution XPS O1s spectra of (a) fluorescent micelles and (b) fluorescent vesicles.

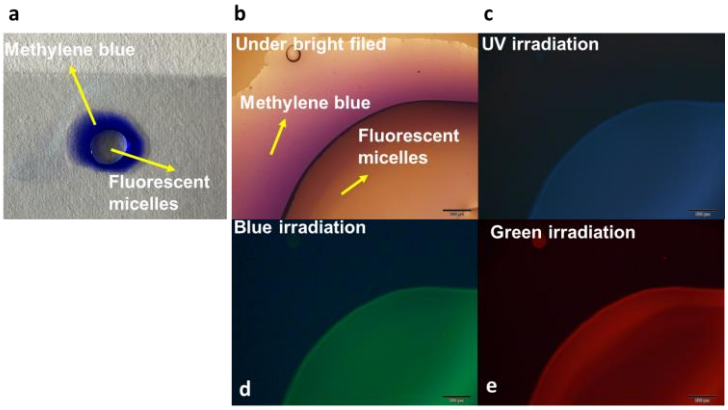

Fig. S15. The pictures of fluorescent micelles added into the methy blue solution under room light (a), under bright field (b), under UV irradiation (c), under blue irradiation (d) and under green irradiation (e).

In order to further demonstrate the hydrophilicity of the fluorescent micelles, we directly added the fluorescent micelles to methyl blue solution (water-soluble dye). It can be observed that the fluorescent micelles are suspended on the methyl blue solution totally, showing high hydrophobicity (Fig. S15a). The solution further observed by fluorescence inverted microscope. Only the fluorescent micelles show blue, green and red fluorescence color under different fluorescent channels, and the methyl blue solution was not fluorescent (Fig. S15b-e). This phenomenon demonstrates that the no fluorescent micelles diffused into the methyl blue solution, due to the fluorescent micelles not soluble in water, which is consistent with other characterization results.

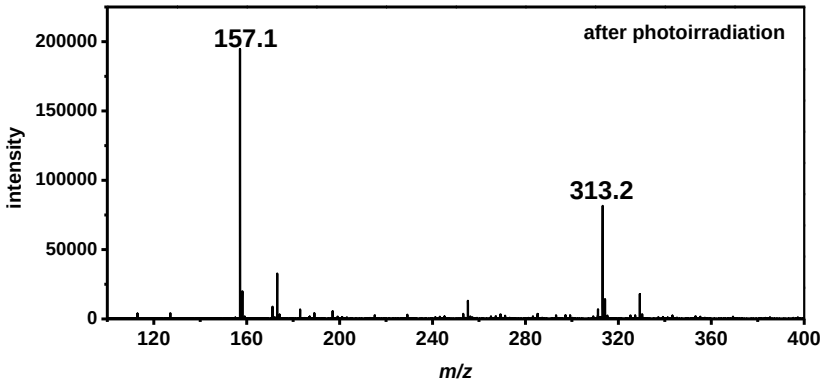

Fig. S16. Mass spectrum of NA after photochemical reaction. The peaks indicate unreacted NA (157.1 m/z) and NA-NA dimer (313.2 m/z), respectively.

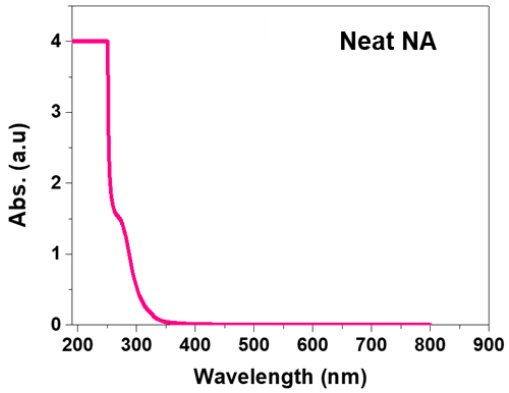

Fig. S17. UV-vis spectrum of neat NA.

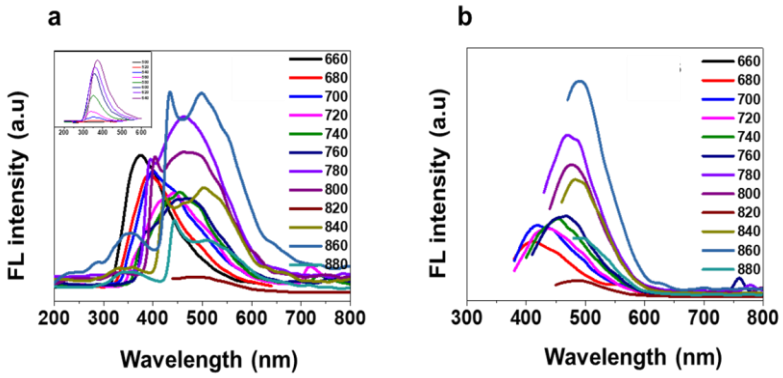

Fig. S18. Fluorescence spectra showing up-conversion of **(a)** fluorescent micelles and **(b)** fluorescent vesicles.

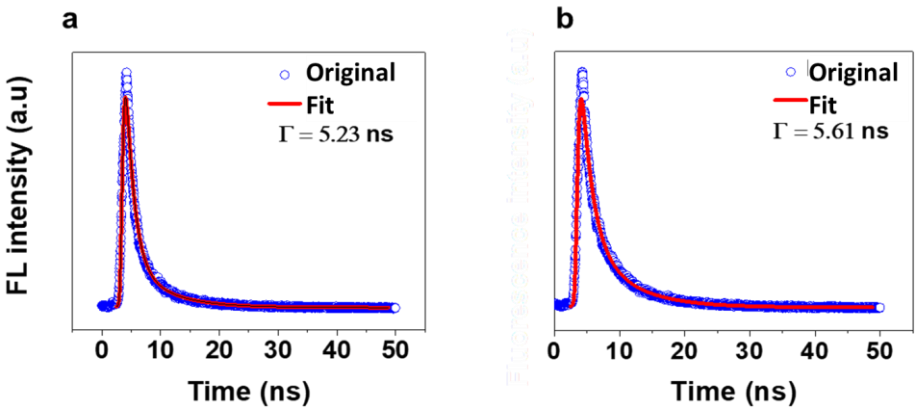

Fig. S27. UV-vis spectra of fluorescent vesicles obtained from different photoirradiation time.

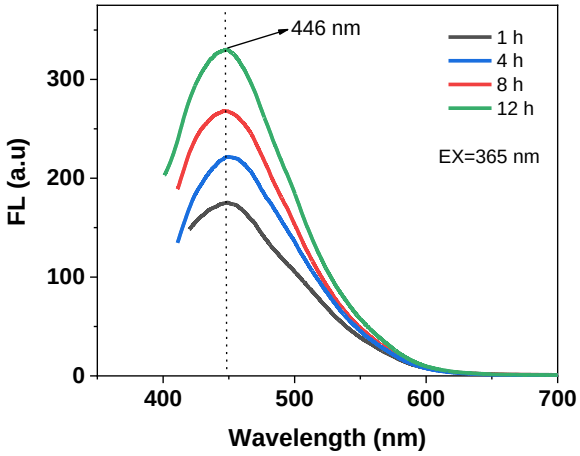

Fig. S19. (a) & (b) FL decay spectra at the excitation of 375 nm and emission of 450 nm, blue lines represent experimental data and red line represent fitted data and corresponding lifetime values are displayed inside each graph.

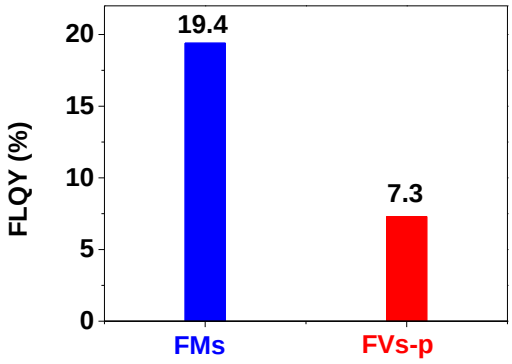

Fig. S20. The fluorescence quantum yields (FLQYs) of fluorescent micelles and vesicles.

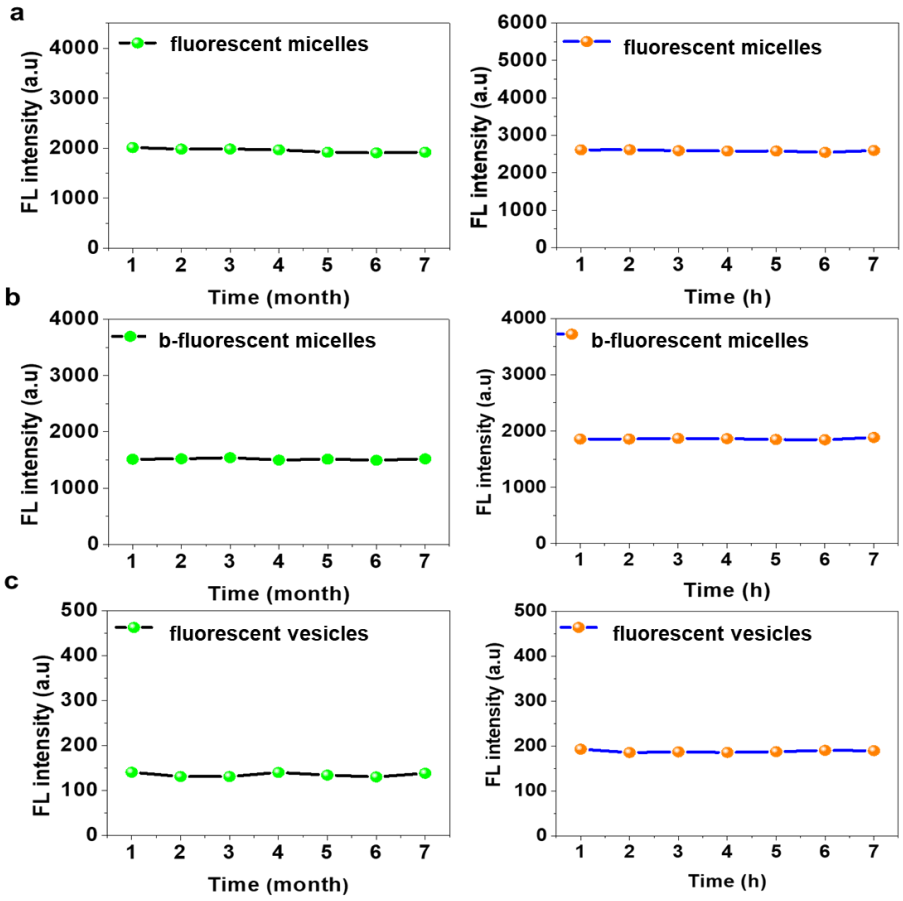

Fig. S21. FL stability of **(a)** fluorescent micelles, **(b)** b-fluorescent micelles and **(c)** fluorescent vesicles under long time daylight (left) and 365 nm UV light (right) irradiation.

Fig. S22. Image of car drawn by fluorescent micelles and treated by water.

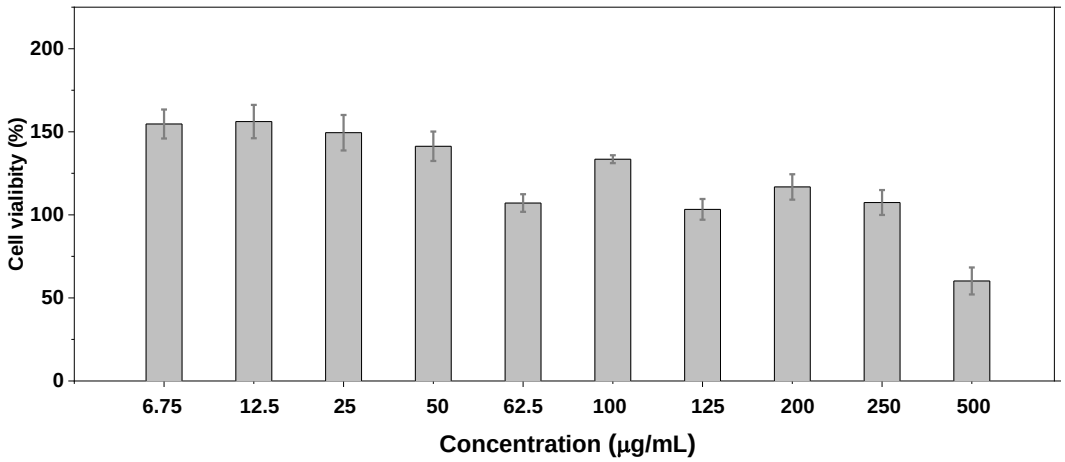

Fig. S23. The viability of A549 cells after incubation for 24 h with different concentrations of fluorescent vesicles, which are evaluated by MTT assay.

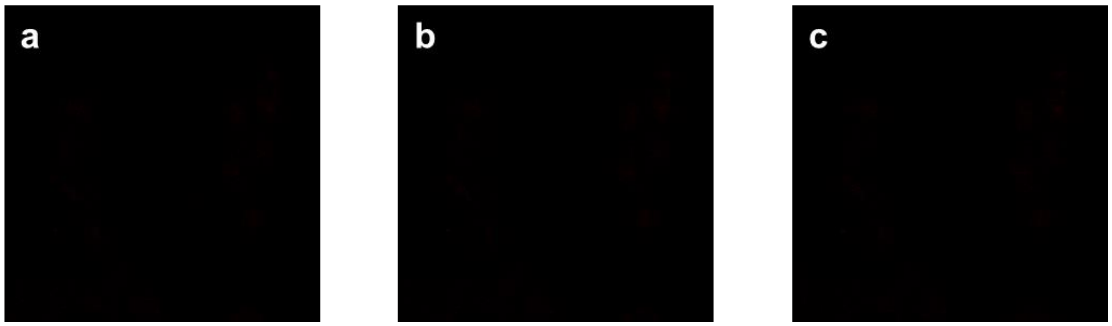

Fig. S24. Cell imaging of control groups. Images of A549 cells without being incubated with fluorescent vesicles excited at **(a)** 408 nm, **(b)** 488 nm, and **(c)** 561nm.

The mechanism for the FVs entering the nucleus:

The unique nuclear-staining may be attributed to the following reasons: First, the unique structured FVs enable nuclear-staining imaging. Second, because of their perfect hydrophilicity, FVs are easily dispersed in physiological environments or aqueous media and transferred into the cells. [7, 8] Third, the amphiphilicity of the vesicles allows FVs to move easily across the amphiphilic plasma and nuclear membrane. Fourth, their low cytotoxicity allows FVs to reach the nucleus and emit FL.

Effects of illumination time on vesicles and FCNs

Fig. S25 shows that the turbidity of the reaction liquid tends to increase gradually as the illumination time is from 1 h to 12 h, meaning the increased number of vesicles. MS result also presents an increased trend of vesicles formation with the prolongation of time, and mainly composed of NA dimers (Fig. S25, S26). It can be concluded that the illumination time only affects the yield of vesicles and has no impact on their structures. Subsequently, the vesicle solutions obtained after different illumination time were further subjected to rotary evaporation for 2 hours. Then, fluorescent vesicles were collected from the aqueous phase after shaking the acquired final yellow liquid with additional water. The absorption spectra of vesicles at 410 nm slightly increase with the increasing of illumination time (Fig. S27). Meanwhile, the intensity of fluorescence emission located at 446 nm increases upon extension of time under 365 nm irradiation, suggesting the increased number of FCNs (Fig. S28). All the samples display almost the same excitation-dependent fluorescent emission, showing the consistence of the generated fluorescent vesicles under different photoirradiation time (Fig. S29). TEM shows that the average dimeters of FCNs are 4.74, 4.87 and 4.80 nm after 1 h, 5 h and 12h irradiation time, respectively (Fig. S31). These results demonstrate that the time of photo-irradiation has no obvious effect on the particle size of FCNs. Their fluorescence quantum yields present a slight increase (Fig. S30), may arising from the increased oxidation degree of FCNs introduced by the increased photoirradiation time, which is consistent with the literature reports.[9]

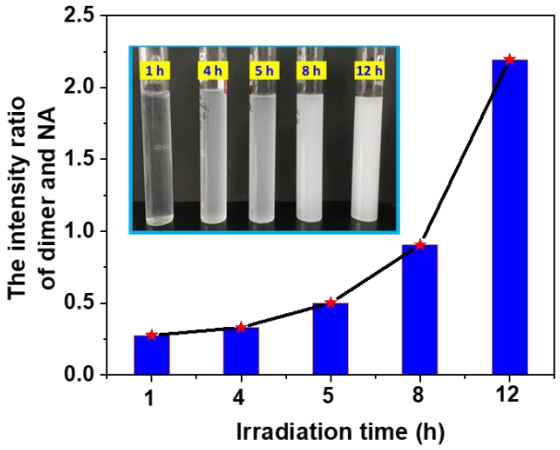

Fig. S25. The intensity ratio of dimer/NA obtained from mass spectra analysis, showing the increasing of dimer upon prolonging the time of photoirradiation. The insert is the corresponding photos showing the samples after different photoirradiation time.

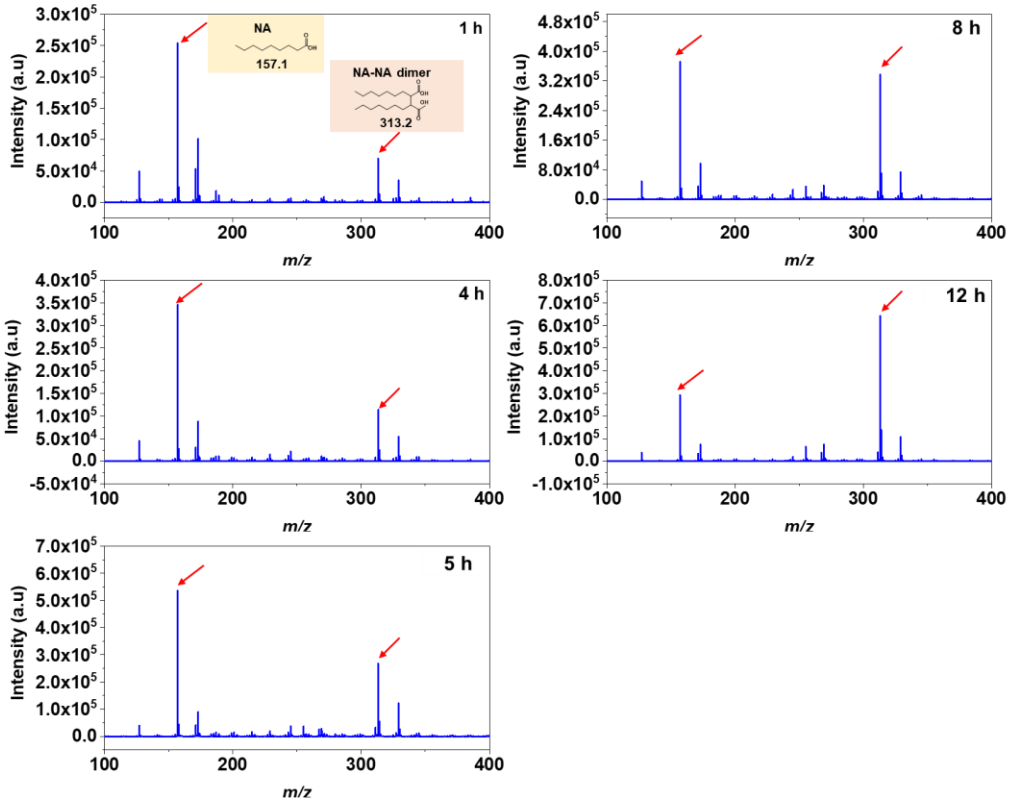

Fig. S26. Vesicles obtained from different photoirradiation time analyzed by the mass spectra under negative mode.

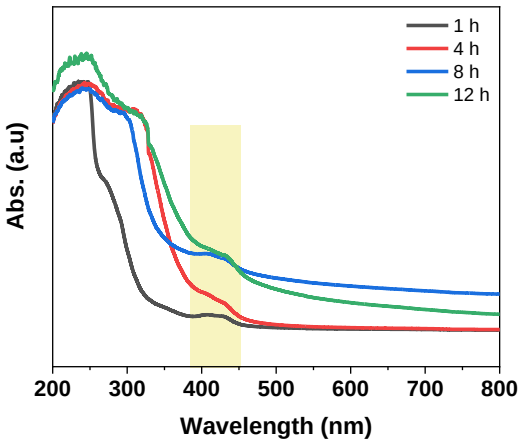

Fig. S28. Fluorescence emission under excitation of 365 nm of vesicles obtained from different photoirradiation time.

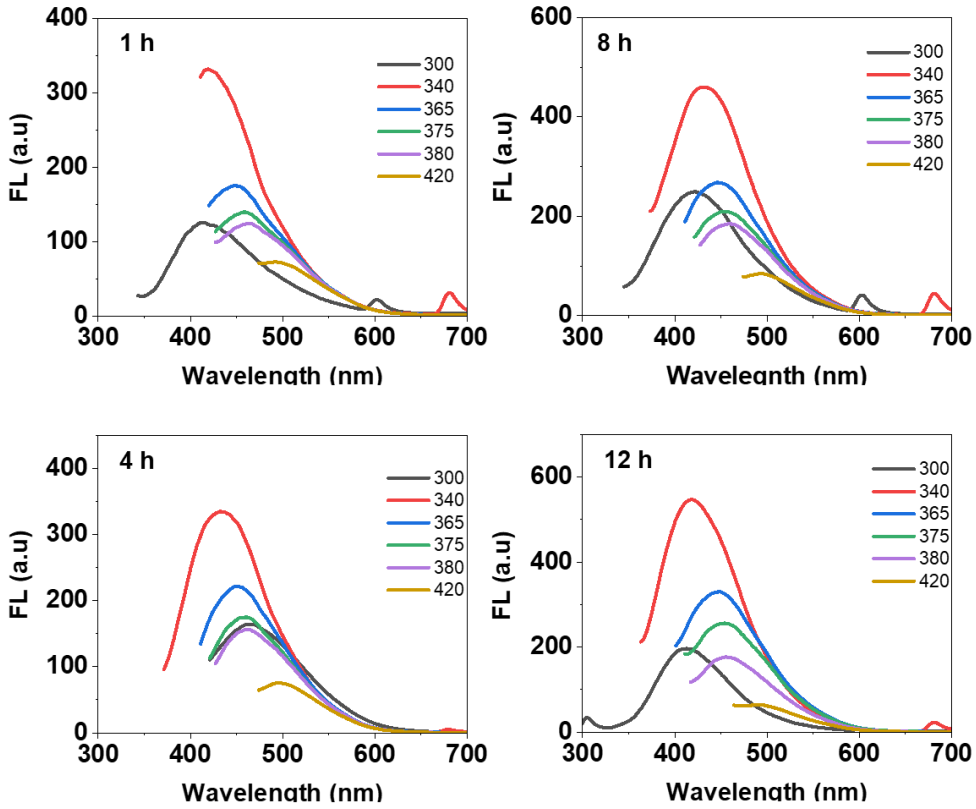

Fig. S29. Fluorescence emission of fluorescent vesicles obtained from different photoirradiation time with excitation from 300 to 420 nm.

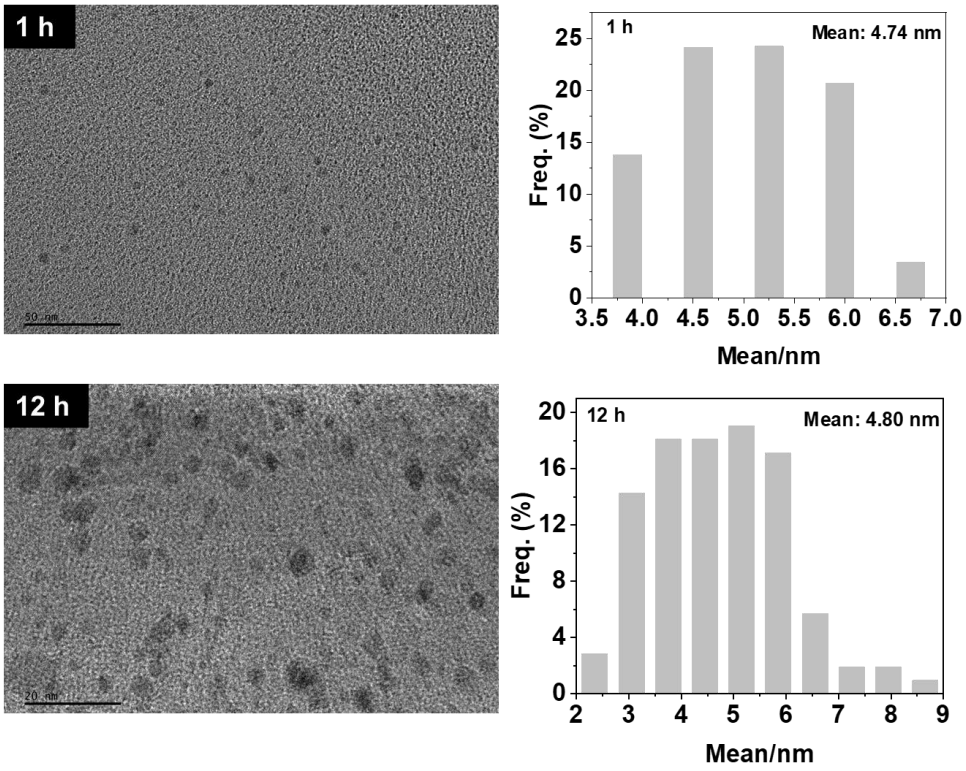

Fig. S30. Size distribution of FCNs on fluorescent vesicles obtained from 1 h and 12 h irradiation.

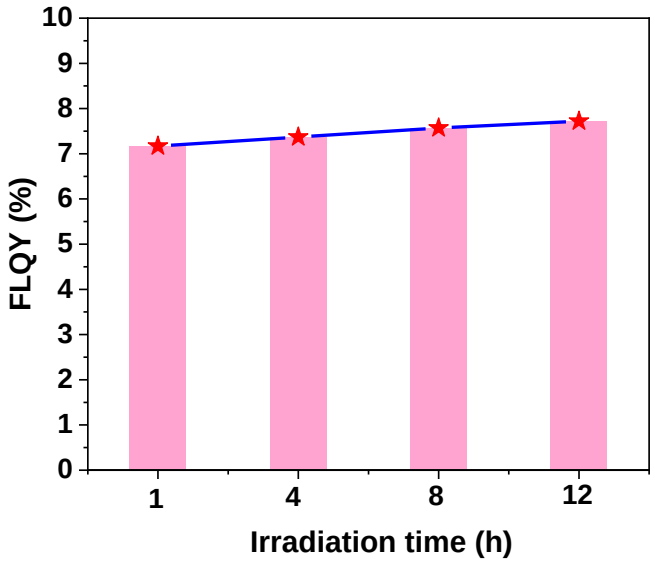

Fig. S31. Fluorescence quantum yield (FLQY) of fluorescent vesicles obtained from different photoirradiation time.

Table S1. The FL lifetime of three fluorescent nanocomposites.

	f_i (%)	f_i (%)	T_i (ns)	T_i (ns)
fluorescent micelles				
1	54.531	0.813	1.422	0.010
2	45.469	1.415	6.262	0.003
b-fluorescent micelles				
1	0.793	0.793	1.426	0.010
2	1.430	1.430	5.976	0.003
fluorescent vesicles				
1	44.205	0.710	1.747	0.010
2	55.795	1.742	6.293	0.002

Average lifetime was calculated according to the formula: $\tau = \frac{f_1\tau_1^2 + f_2\tau_2^2}{f_1\tau_1 + f_2\tau_2}$

Table S2. Fluorescence quantum yields **(**FLQYs) of three fluorescent nanocomposites and quinine sulfate.

sample	Integrated emission intensity(I)	Abs. (A)	solvent	Refractive index of solvent (25 ºC)	FLQYs (%)
quinine sulfate	510.251	0.04691	0.5 M H_2SO_4	1.33	54
fluorescent micelles	323.314	0.05626	ethanol	1.096	19.4
b-fluorescent micelles	303.963	0.05553	ethanol	1.096	18.5
fluorescent vesicles	80.623	0.05465	water	1.33	7.3

$$\phi = \phi_R \times \frac{I}{I_R} \times \frac{A_R}{A} \times \frac{\eta^2}{\eta_R{}^2}$$

Φ Where is the quantum yield, I is the measured integrated emission intensity, η is the refractive index, and A is the optical density. The subscript R refers to the reference fluorophore of known quantum yield.

References

1. C. G. Palivan, R. Goers, A. Najer, X. Zhang, A. Car and W. Meier, *Chemical Society reviews*, 2016, **47**, 377-411.
2. Y. F. Kang, Y. W. Fang, Y. H. Li, W. Li and X. B. Yin, *Chemical communications*, 2015, **51**, 16956-16959.
3. G. Eda, Y. Y. Lin, C. Mattevi, H. Yamaguchi, H. A. Chen, I. S. Chen, C. W. Chen and M. Chhowalla, *Advanced materials*, 2010, **22**, 505-509.
4. M. Minella, M. Demontis, M. Sarro, F. Sordello, P. Calza and C. Minero, *Journal of Materials Science*, 2015, **50**, 2399-2409.
5. P. Zuo, X. Lu, Z. Sun, Y. Guo and H. He, *Microchimica Acta*, 2015, **183**, 519-542.
6. J. Shen, Y. Zhu, C. Chen, X. Yang and C. Li, *Chemical communications*, 2011, **47**, 2580-2582.
7. X. Zhang, X. Zhang, S. Wang, M. Liu, L. Tao and Y. Wei, *Nanoscale*, 2013, **5**, 147-150.
8. D. Wang, H. Su, R. T. K. Kwok, X. Hu, H. Zou, Q. Luo, M. M. S. Lee, W. Xu, J. W. Y. Lam and B. Z. Tang, *Chemical Science*, 2018, **9**, 3685-3693.
9. L. Bao, C. Liu, Z. L. Zhang and D. W. Pang, *Advanced Materials*, 2015, **27**, 1663-1667.